



# **An Experimental Investigation To Determine Interaction Between Rotating Bodies**

**(MSFC Center Director's Discretionary Fund Final Report,  
Project No. 279–00–16)**

*R.N. Grugel and M.P. Volz  
Marshall Space Flight Center, Marshall Space Flight Center, Alabama*

*K. Mazuruk  
Universities Space Research Association, Huntsville, Alabama*

## The NASA STI Program Office...in Profile

Since its founding, NASA has been dedicated to the advancement of aeronautics and space science. The NASA Scientific and Technical Information (STI) Program Office plays a key part in helping NASA maintain this important role.

The NASA STI Program Office is operated by Langley Research Center, the lead center for NASA's scientific and technical information. The NASA STI Program Office provides access to the NASA STI Database, the largest collection of aeronautical and space science STI in the world. The Program Office is also NASA's institutional mechanism for disseminating the results of its research and development activities. These results are published by NASA in the NASA STI Report Series, which includes the following report types:

- **TECHNICAL PUBLICATION.** Reports of completed research or a major significant phase of research that present the results of NASA programs and include extensive data or theoretical analysis. Includes compilations of significant scientific and technical data and information deemed to be of continuing reference value. NASA's counterpart of peer-reviewed formal professional papers but has less stringent limitations on manuscript length and extent of graphic presentations.
- **TECHNICAL MEMORANDUM.** Scientific and technical findings that are preliminary or of specialized interest, e.g., quick release reports, working papers, and bibliographies that contain minimal annotation. Does not contain extensive analysis.
- **CONTRACTOR REPORT.** Scientific and technical findings by NASA-sponsored contractors and grantees.
- **CONFERENCE PUBLICATION.** Collected papers from scientific and technical conferences, symposia, seminars, or other meetings sponsored or cosponsored by NASA.
- **SPECIAL PUBLICATION.** Scientific, technical, or historical information from NASA programs, projects, and mission, often concerned with subjects having substantial public interest.
- **TECHNICAL TRANSLATION.** English-language translations of foreign scientific and technical material pertinent to NASA's mission.

Specialized services that complement the STI Program Office's diverse offerings include creating custom thesauri, building customized databases, organizing and publishing research results...even providing videos.

For more information about the NASA STI Program Office, see the following:

- Access the NASA STI Program Home Page at <http://www.sti.nasa.gov>
- E-mail your question via the Internet to [help@sti.nasa.gov](mailto:help@sti.nasa.gov)
- Fax your question to the NASA Access Help Desk at (301) 621-0134
- Telephone the NASA Access Help Desk at (301) 621-0390
- Write to:  
NASA Access Help Desk  
NASA Center for AeroSpace Information  
7121 Standard Drive  
Hanover, MD 21076-1320



# **An Experimental Investigation To Determine Interaction Between Rotating Bodies**

**(MSFC Center Director's Discretionary Fund Final Report,  
Project No. 279–00–16)**

*R.N. Grugel and M.P. Volz*

*Marshall Space Flight Center, Marshall Space Flight Center, Alabama*

*K. Mazuruk*

*Universities Space Research Association, Huntsville, Alabama*

National Aeronautics and  
Space Administration

Marshall Space Flight Center • MSFC, Alabama 35812

## **Acknowledgments**

Support of the Center Director's Discretionary Fund at NASA Marshall Space Flight Center is greatly appreciated.

Available from:

NASA Center for AeroSpace Information  
7121 Standard Drive  
Hanover, MD 21076-1320  
(301) 621-0390

National Technical Information Service  
5285 Port Royal Road  
Springfield, VA 22161  
(703) 487-4650

## TABLE OF CONTENTS

1. INTRODUCTION .....	1
2. INITIAL EXPERIMENTS .....	5
3. THEORY OF THE NONAXISYMMETRIC FARADAY DISC .....	7
4. LONG NONAXISYMMETRIC FARADAY DISC .....	10
5. FINITE CYLINDER MODEL .....	13
6. NUMERICAL RESULTS .....	25
7. EXPERIMENTAL RESULTS .....	27
REFERENCES .....	29

## LIST OF FIGURES

1.	High-speed motor assembly as it sits on the microbalance .....	5
2.	Air-powered device designed to rotate a metallic disc, in this case bismuth, at high speeds. Another bismuth disc is seen suspended above the rotating disc .....	6
3.	High-speed brass wheel assembly used in this investigation .....	8
4.	Angular dependence of the $r$ component of the normalized magnetic field. The field is calculated at the surface of the disc for a set of 11 $q$ values .....	11
5.	Dependence of the $r$ component of the normalized magnetic field on the skin depth parameter, $q$ , for several angular positions: 0, 0.5, 1, 1.5, 2, and $p$ , in radians .....	12
6.	The streamlines of the total magnetic field for a set of the $q$ values: 1, 3, 5, and 10. The external magnetic field goes from left to the right, and the wheel rotates counterclockwise. As the speed increases, the magnetic field is repelled from the wheel .....	12
7.	Schematic of the geometry and the cylindrical coordinates .....	13
8.	A set of six functions of $r$ and $z$ variables that represent the magnetic field in the spinning cylinder: (a) $\text{Re}(B_r)$ , (b) $\text{Im}(B_r)$ , (c) $\text{Re}(B_j)$ , (d) $\text{Im}(B_j)$ , (e) $\text{Re}(B_z)$ , and (f) $\text{Im}(B_z)$ . Re is the real part and Im is the imaginary part .....	25
9.	$B_r/B_0$ as a function of the skin depth parameter, $q$ . Values are taken at the middle of the rim .....	26
10.	$B_\phi/B_0$ as a function of the skin depth parameter, $q$ . Values are taken at the middle of the rim .....	26
11.	Experimental values (black circles) and the corresponding theoretical fit (hollow circles) assuming that the electrical conductivity is $43 \text{ n}\Omega\text{m}$ .....	27

## LIST OF TABLES

1.	Measured electrical resistivities for several brasses .....	28
----	---	----

## NOMENCLATURE

$A_n$	coefficient
<b>B</b>	magnetic field
$B$	magnetic field strength
$B_0$	external magnetic field
<b>C</b>	vector
$C$	coefficient
<b>D</b>	vector
$D$	coefficient
$d$	coefficient
<b>E</b>	electric field, matrix
<b>e</b>	unit vector
$e$	Euler number
<b>F</b>	vector
$F_n$	coefficient
$f$	scalar
$G_n$	coefficient
$I$	coefficient
<b>J</b>	electric current density
$J$	scalar
$L$	height

## NOMENCLATURE (Continued)

<b>M</b>	matrix
$M_{m,n}$	matrix elements
$m$	integer
<b>N</b>	matrix
$n$	integer
$p$	coefficient
$q$	skin depth parameter
Re	real value
<b>r</b>	radius vector
$r$	radius
<b>S</b>	surface
$s_n$	coefficient
$T_{m,n}$	matrix element
$t_n$	coefficient
<b>U</b>	matrix
$U_{m,n}$	matrix element
$u$	potential
<b>V</b>	matrix
<b>v</b>	velocity of the medium
$z$	coordinate
$\beta_n$	roots of <b>J</b>

## NOMENCLATURE (Continued)

$\delta$	Kronecker delta function
$\varepsilon$	coefficient
$\Phi$	scalar potential
$\gamma_n$	coefficient
$\varphi$	angular coordinate
$\kappa$	coefficient
$\lambda_n$	coefficient
$\mu$	magnetic permeability
$\rho$	radius coordinate
$\sigma$	electrical conductivity
$\omega$	angular/rotational velocity
$\partial$	derivative operator
$\nabla$	Nabla operator

## TECHNICAL MEMORANDUM

### **AN EXPERIMENTAL INVESTIGATION TO DETERMINE INTERACTION BETWEEN ROTATING BODIES (MSFC Center Director's Discretionary Fund Final Report, Project No. 279-00-16)**

#### **1. INTRODUCTION**

Present physical theories, both phenomenological and quantum, while in a broad agreement with experimental evidence, on a deeper level of logical analysis, encounter many inconsistencies or problems. Although these problems have no immediate practical consequences, they stimulate the search for new fundamental models of reality. Very active areas are now superstring theories, geometrodynamics extensions of general relativity, such as Kaluza-Klein theories, topological geometrodynamics theories, and twistor or torsion field theories. This new theoretical breeze brings new challenges to experimentalists.

As our quest for better understanding of the physics governing nature continues and more experimental data became available, we begin to see some remarkable similarities between the macrocosm and microcosm. Perhaps the most important is the rotational motion of matter at any length scale. Planets, stars, galaxies, and clusters of galaxies are all spinning objects, and at the microscopic level, all the elementary particles ( $\approx 1,000$ ) are spinning entities. Consequently, we witness that matter spins at all scale levels. If one assumes a spinning distribution of electric charges than are in accord with the law of induction, a magnetic dipole will result. Although such a classical model cannot be directly translated into the microworld, the general cause for the phenomenon of the magnetic moment remains the same.

The magnetic moment of the particles is further related to its spin through the gyromagnetic constant, and theoretical predictions for this parameter are in excellent agreement with experimental data. However, there is mounting evidence on both the microlevel and macrolevel that our physical model of spinning objects needs to be reassessed. Many of the theories mentioned above and models of particles as nonsingular extended objects, usually based on classical electrodynamics, point to the existence of some new types of interactions. Some of these theories, while maintaining the essence of the classical physics as a subset, predict interaction between spinning macroscopic bodies. Also, reports exist of experiments, conducted over the last hundred years, that point to such phenomena. It is difficult to assess the credibility of these data since others have not repeated the experiments.

The new paradigm in physics revolves around the concept of vacuum and/or multidimensional geometry. Our commonly accepted understanding of the vacuum is based on the Dirac sea of particles. Here the energy spectrum of the particles has a gap and the lower energy band is almost fully occupied. When a particle acquires sufficient energy, it is transferred from the lower to the upper energy band. A free particle is created this way, and a hole is left in the lower band that represents an antiparticle. From the quantum principle of uncertainty, there will always be some fluctuations in the system. This means

that the vacuum actually constitutes a complex fluctuating field of various particles. Wheeler<sup>1</sup> evokes that this particle flux has an energy density on the order of  $10^{94}$  g/cm<sup>3</sup>. The Casimir force, recently measured,<sup>2</sup> that acts between two electrically conducting bodies confirms the viability of a vacuum as a real medium. In short, the physical properties of a vacuum depend on the presence and strength of macroscopic electrical, magnetic, and gravitational fields.

Spin is the fundamental property of elementary particles. For example, neutrons, electrically neutral particles, have a spin of  $\hbar/2$ , as do electrons. Many of the modern quantum and classical theories also consider the physical vacuum as having spin or torsion properties. If so, then some macroscopic manifestation similar to the Casimir force would be present. Modification of the local vacuum spin properties by electromagnetic fields or by rotating bodies is then possible. However, no a priori estimates of the effect can presently be made because the current vacuum models are inadequate.

Scientists in the 19th century liked to consider the free space between bodies as a medium with fluid-like properties so spin can be transmitted. Beginning early this century many investigations have been conducted with the intent of establishing an influence of solid body rotation on electrical, magnetic, and gravitational properties. Einstein, recognizing that rotational motion was not correctly treated in his first general relativity theory, proposed, with Cartan, the first gravitational theory of spinning bodies in 1923.<sup>1</sup> Briefly, this general relativity theory, in its classical formulation, predicts a small correction to the Newtonian gravitational force for spinning macroscopic masses. This correction is rather difficult to detect under presently achievable rotational speeds. Several new proposed superstring models dealing with reconciling gravity and quantum theory point to bigger effects. Also, twistor or spinor theories, comprising natural extensions of the general relativity, assume the existence of additional forces between the spinning bodies of unspecified magnitude that can only be determined experimentally. Some experiments were reported decades ago with no definite claims, and only a few measurements have been recently attempted. Also, we want to emphasize that there are several ways rotational motion can be included into the general relativity theory, as attested to by many later models, that address the necessary existence of gravitomagnetic fields.<sup>3-8</sup>

Although clearly overshadowed by theory, there have been some limited experimental works conducted in this area. Myshkin<sup>9,10</sup> conducted a series of experiments purported to discover a relationship between macroscopic fields and rotation. Experiments utilizing gyroscopes that have not received much exposure were later performed in the U.S.S.R. by Kozyrev.<sup>11</sup> Other obscure Russian literature on experiments and theories related to non-newtonian mechanics includes the following:

- Spartak Poliakov's book with experiments on complex gyroscopic systems that exhibit non-newtonian behavior.
- A theoretical book by Gerlovin, whose approach is based on Einstein's general relativity theory, that extends the dimensions of the world from four to seven. He obtains a spectrum of the elementary particles, rest masses, and life times that agree with existing data reasonably well (six digits or so). His approach is partially based on his discoveries that some classical orbits of the point-like charges could be nonradiative; similarities with the string theories are also evident. He also predicts some unknown gravity-related phenomena.

- Veinik's book addresses thermodynamics of real processes. He describes his experiments on gyroscopes as well as on torsion pendulums, the effects of which are not easily explainable by existing mainstream physics.
- Shipov's book relates his ideas on torsion fields. Mathematically his book is sound; whether his theoretical model is applicable to the real world remains to be seen, but his ideas attract some of the best scientists in the field.

A detailed experimental study that suggests a possible force between spinning bodies has been conducted by two physicists from Japan and reported in great detail in *Phys. Rev. Lett.*<sup>12</sup> In short, a small incremental decrease in weight was detected by a chemical balance as a function of increasing the gyroscope's rotation rate in a clockwise direction. Curiously, there was no effect observed when rotating counterclockwise. Subsequent experiments conducted in the United States,<sup>13</sup> utilizing a very precise gyroscope, did not find any weight changes.

A French group<sup>14</sup> did record a change, albeit 20 times smaller than that observed by the Japanese group. Here it is relevant to state that the United States and French teams used different types of gyroscopes and did not accurately reproduce the Japanese experimental conditions. It has been conjectured that the effects observed by the Japanese were due to vibrations of the gyroscope rotor that utilized average quality ball bearings.<sup>15</sup> In view of this premise, it is now interesting to compare the results with those of the Russians<sup>11</sup> who, independent of the Japanese, also used a chemical balance to measure gyroscope weight as a function of rotation. Initially, to within six significant figures, they did not see any weight changes. However, upon intentionally introducing small vibrations into the shaft, the weight of the gyroscope was affected in the fourth digit and only in one rotational direction, as in the Japanese study. The gyroscope was suspended on a rubber strip to suppress propagation of vibrations to the balance; this provision did not affect the observed phenomenon. In support of the above observations, Shipov<sup>16</sup> theoretically shows that nonsymmetric rotation is necessary to generate a change.

The same Japanese team recently measured the free fall of gyroscopes in a vacuum tube. They again observed a reduction of the acceleration for clockwise-rotating gyroscopes. There has also been one report (apparently not refereed) of an experiment conducted in the United States<sup>17</sup> of freely falling gyroscopes in which the authors claim to observe changes in drop velocity due to the imposed rotation.

The above studies utilized measurements based on rotating objects. Consider now the series of very well-planned experiments (that passed considerable critical review) elegantly conducted by Brush in the early 1920s.<sup>18-20</sup> After an introduction that evokes the essence of string theory, he considers simple motion of pendulums and drop velocities of different metals (zinc, bismuth, and lead) fashioned to have the same weight, dimensions, and centers of mass. Invariably the denser metal swung or dropped faster, a direct contradiction to the established laws of physics. He concludes that there is something intrinsic to materials themselves, making particular note of the peculiar behavior of bismuth.

Bismuth is not a typical metal. In contrast to most, it expands upon freezing. Bismuth is the most diamagnetic of all metals and only mercury has a smaller thermal conductivity. It has high electrical resistance and the greatest increase in electrical resistance when placed in a magnetic field; i.e., magnetoresistance. Finally, bismuth has 209 nucleons, the largest of any stable element. These characteristics bring to mind Wallace's detailed patents.<sup>21-23</sup> In short, Wallace, while at General Electric, invented

a machine that spun a mass to promote nuclear spin alignment. This, in turn, generated a secondary gravitational field that he called a kinnemassic field; i.e., a gravitomagnetic field. It was necessary, or perhaps optimal, for the spinning mass to have an odd number of nucleons. Wallace employed a brass wheel, although he notes bismuth to be preferable. To the best of our knowledge, outside of Wallace's results, there were no subsequent studies (at least published) confirming or denying his claims. This has been a point of numerous speculations.

We note that many researchers, apparently independent of each other, have conducted experiments that imply the existence of unusual forces due to rotation and/or electric/magnetic field interactions. These efforts are still met with some skepticism by the scientific community. We have, consequently, fashioned our initial experiments after them.

## 2. INITIAL EXPERIMENTS

Our preliminary experimental work is patterned after some earlier efforts, primarily those conducted in Japan that reported a small incremental decrease in a gyroscope's weight as a function of increasing its rotation rate in a clockwise direction,<sup>12</sup> and those of Wallace<sup>21-23</sup> conducted in early 1970s that consisted of spinning a brass wheel.

In contrast to the Japanese experiment that utilized gyroscopes, our work consisted of placing a small, high-speed electric motor directly onto the plate of a microbalance. The general setup can be seen in figure 1. Our experiments took a number of progressions. Initially, to reduce vibrations, insulating foam was wrapped around the motor. Shortly after initiating rotation (up to 30,000 rpm), a reduction of weight was detected that, upon stopping, did not return. Initially surprising, we soon came to realize the heat of the motor had vaporized some of the insulation with which it was in contact. Subsequently, the insulation was removed and the motor suspended in a plastic laboratory bottle. When the motor was spun in this configuration, a small decrease in weight ( $\approx 20$  mg) was again detected. In contrast to our first attempt, the weight returned after rotation ceased, and the result was reproducible. However, upon sealing the motor in the bottle (fig. 1), initiation of rotation produced no decrease in weight. A simple calculation showed that if heating from the motor slightly increased the local air temperature, the change in density could account for the observed weight loss. The above experiment is not exactly like the Japanese effort but is valuable in pointing out the care needed in taking and, in particular, assessing measurements.



Figure 1. High-speed motor assembly as it sits on the microbalance.

A mechanical, air-driven device to promote rapid rotation (up to 20,000 rpm) of a metal disc (in this case bismuth) was also constructed (fig. 2) and used to conduct experiments. The first experiment consisted of spinning the disc in the presence of the Hall probe with the intent of detecting a change in the adjacent magnetic field; none was detected. The second experiment focused on determining if rotation of the disc would influence movement of another disc. Here, a second bismuth disc (fig. 2) was suspended  $<1$  mm above the rotating disc; a plastic film was placed between the two to eliminate convection effects. A mirror was attached to the suspension wire on which a laser beam was shown and reflected onto the adjacent wall. Thus, a very sensitive means of detecting any motion of the suspended disc was ensured. The lower bismuth wheel was then accelerated to high rpm while the reflected laser beam was observed. After numerous tries and variations, it was concluded that the lower rotating wheel did not influence the upper suspended wheel. The results, or perhaps more accurately nonresults, led to our third experimental investigation in which a spinning brass disc was utilized.

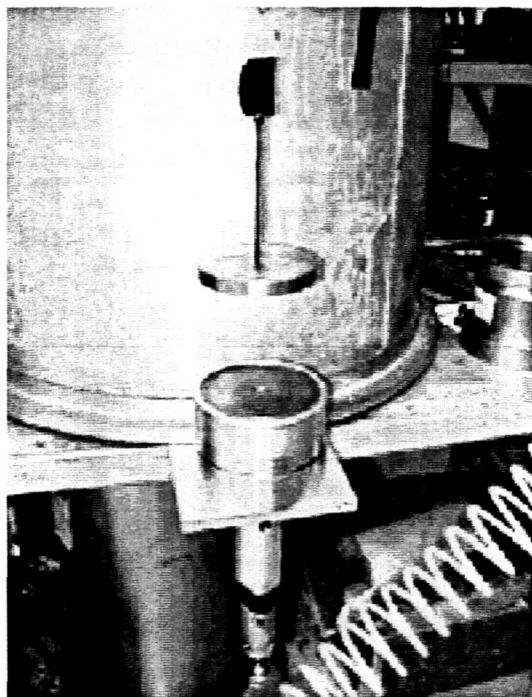


Figure 2. Air-powered device designed to rotate a metallic disc, in this case bismuth, at high speeds. Another bismuth disc is seen suspended above the rotating disc.

### 3. THEORY OF THE NONAXISYMMETRIC FARADAY DISC

The Homeopolar machine, or so-called Faraday disc, is perhaps the simplest example of a spinning body in presence of a magnetic field. It consists of a metallic disc with a static magnetic field applied along the axis. When rotated, a voltage across the radius of the disc is generated. This was the crucial experiment, performed more than 150 yr ago, in discovering the induction principle of electrodynamics. Since then many attempts were made to refine our understanding of its underlying mechanisms, and discussion of this matter is still continuing.

One of the unresolved questions is whether there is an additional degree of freedom for the magnetic field. Consider, as an example, an axisymmetric magnetic field induced by a permanent magnet. Now, let the magnet spin around its axis. This prompts the question of what happens to the magnetic field. Do the magnetic field lines rotate as well, or is it just magnet motion that has no consequence to the magnetic field? Several clever experiments have been proposed, but doubt still percolates through the relevant literature. Consequently, there is growing interest in fundamental research on possible unknown effects induced by spinning of macroscopic bodies. For example, we note the torsion balance experiments by the Eöt-Wash Group at the University of Washington<sup>24</sup> looking for new short-range interactions, existing in accordance to some recent theoretical speculations. Gravity probe-B experiments by NASA will accurately measure rapidly spinning spheres in space with the aim of investigating gravitomagnetic effects predicted by Einstein's general relativity.

Our initial interest, which led to this work, stemmed from the ideas of Wallace that were presented in a series of the U.S. patents.<sup>21-23</sup> Wallace, while at General Electric, investigated a rapidly spinning brass wheel and conjectured the existence of a novel field. No further work was done to confirm or deny his claims. Experimentally, a brass wheel 8.6 cm in diameter and 1.88 cm in thickness was rotated up to 28,000 rpm and a faint signal measured by a Hall probe was detected at a distant point. In an attempt to explain his results, he pointed to spin interactions. A convenient way to describe the direct spin-spin interactions between the spin-polarized beams of particles and the target is by introducing the concept of pseudomagnetism, an idea similar to the Weiss molecular. Our hypothesis is that pseudomagnetism can explain Wallace's observations.

In our setup, we avoided the use of any magnetic material and spun a 4-in-diameter, 1.4-in-thick brass wheel by an air turbine. Furthermore, we shielded our system from interference with Earth's magnetic field (fig. 3).

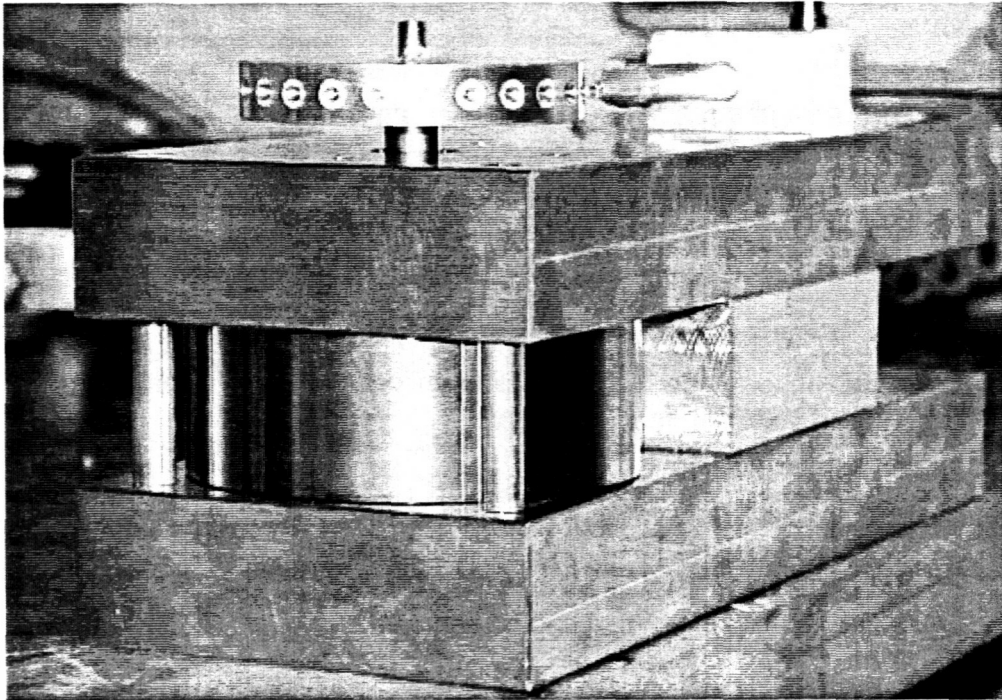


Figure 3. High-speed brass wheel assembly used in this investigation.

To detect a possible but unknown field (gravitomagnetic), we used both the Hall probe and a much more sensitive giant magnetoresistive sensor. Within our sensitivity limit ( $10^{-4}$  G) and a rotation rate of 8,000 rpm, no signal was detected. However, with no magnetic shielding, a strong signal, its magnitude increasing as the rotational speed increased from zero, was measured at the rim of the wheel. Unexpectedly, the signal went through a peak value and began dropping down as the rotation rate increased further, even passing through the zero value. For this effect to happen, the Earth's magnetic field would have to be orthogonal to the axis of the wheel. This configuration is nontypical for Faraday disc studies, and no relevant literature was found.

In an effort to understand the phenomenon within the frame of magnetohydrodynamics, a theoretical model of a very long cylinder was developed that qualitatively reproduces the effect. In essence, the explanation is as follows. Consider an arrangement of a wheel with its axis positioned horizontally in a vertical magnetic field. When the wheel begins to spin, an electric current is induced in it that, in turn, induces a magnetic field that is in a horizontal direction. Now, the total magnetic field will be in a nonvertical direction. As the speed of the wheel increases, the induced magnetic field will become nonhorizontal. Specifically, it will have an upward vertical component. Now the induced current will be orthogonal to the sum of the external and induced magnetic field, triggering further rotation. This self-consistent treatment will result in an upward drift of the direction of the maximum of the induced magnetic field. To conclude, as the speed increases, the magnitude of the induced magnetic field increases and the direction of the maximum shifts upward. The detector placed along the horizontal line crossing the wheel axis will initially display a signal buildup due to an increase of the magnitude of the induced magnetic field. Then, when the magnitude of the field increases, the maximum shifts from the horizontal to the vertical position, resulting in a signal drop.

Here we would like to comment on the Wallace experiments. The faint signals he observed could result from a lack of magnetic shielding. Use of a steel base and support bars is a potential source for measurements to be contaminated by parasitic magnetic fields. Although we did not reach his 28,000-rpm level, our disc is markedly bigger and the detection system is more sensitive. Moreover, the sensor is based on alignment of the nuclear spins, and should be preferable to the measurements of spin-spin interactions.

In this work, we developed a theoretical model of a nonaxisymmetric Faraday disc. First, we formulate an analytical model of an infinitely long, rotating cylinder in the magnetic field orthogonal to its axis. This model has its own merit as it clearly demonstrates the basics of the observed phenomena. The second is a finite cylinder model. Essentially, it is a semianalytical model. However, it allows for very good approximate analytic solutions. The presented solution could, for example, be used as a benchmark for numerical magnetohydrodynamic modeling. We note here that the considered model, due to its simple geometry, is a basic magnetohydrodynamic problem related to dynamo theory. Finally, in the last section, we present our experimental data and compare it with the proposed theory.

#### 4. LONG NONAXISYMMETRIC FARADAY DISC

In this section we develop a simple analytical model of an infinitely long, rotating metallic cylinder in the presence of a uniform magnetic field orthogonal to the cylinder's axis.

The basic equations of this magnetohydrodynamic model are well known and are given for completeness in section 5. As a natural choice, we utilize a cylindrical coordinate system, with the wheel axis corresponding to the  $z$  axis; we do not have the  $z$  component of the induced magnetic field. Furthermore, an angular dependence is harmonic with only one basic component. This allows one to introduce a complex representation of the magnetic field that could be related to the experimental value through this particular choice:

$$B^{(\text{exp})} = \text{Re}[B(r)\text{exp}i\phi] . \quad (1)$$

For the  $r$  component, the governing equation reads

$$\left( \frac{\partial^2}{\partial r^2} + \frac{3}{r} \frac{\partial}{\partial r} \right) B_r = i\mu\sigma\omega(B_0 + B_r) , \quad (2)$$

where  $B_0$  is an external magnetic field,  $\omega$  is the angular velocity,  $\mu$  is the magnetic permeability, and  $\sigma$  is the electrical conductivity.

The solution of this equation can be expressed through Bessel functions and is

$$B_r = -B_0 + CJ_1(qr)/r , \quad (3)$$

where  $q^2 = -i\mu\sigma\omega$ , and the corresponding expression for the  $B_\phi$  component is

$$B_\phi = -iB_0 - iCJ_1(qr)/r + iCqJ_0(qr) . \quad (4)$$

In the free space around the cylinder, the induced field is given by

$$B_r^{\text{space}} = C'/r^2, \quad B_\phi^{\text{space}} = -iC'/r^2 . \quad (5)$$

In this work, we do not consider magnetic materials, so the magnetic permeability is assumed uniform throughout the region. This implies that the magnetic field is continuous across the boundaries and we obtain for unknown coefficients  $C$  and  $C'$ :

$$C = \frac{2B_0}{qJ_0(qr_0)}, C' = -B_0r_0^2 + 2B_0 \frac{J_1(qr_0)}{qr_0J_0(qr_0)}. \quad (6)$$

Then for the value of the  $r$  component of the induced magnetic field at the surface, we obtain

$$B_r(r_0) = -B_0 + \frac{2B_0J_1(qr_0)}{qJ_0(qr_0)r_0}. \quad (7)$$

Utilizing equations (7) and (1) we can plot the induced  $r$  component of the normalized magnetic field, at the surface as a function of the angular coordinate for a set of  $q$  values. The corresponding plot is presented in figure 4.

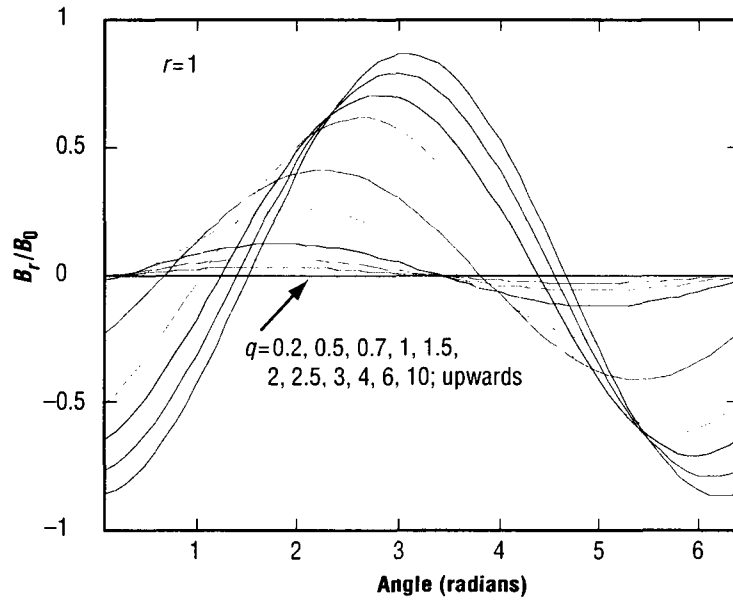


Figure 4. Angular dependence of the  $r$  component of the normalized magnetic field. The field is calculated at the surface of the disc for a set of 11  $q$  values.

A plot of the  $r$  component of the magnetic field at various angular positions as a function of angular velocity is depicted in figure 5. This graph can be directly compared with the experimental data. The bottom curve corresponds to the direction of the external magnetic field,  $\phi=0$ . Then the sequential values for the angles are 0.5, 1, 1.5, 2, and  $\pi$  (in radians). The value of 1.5 corresponds to the horizontal sensor position and was used in most of the experiments.

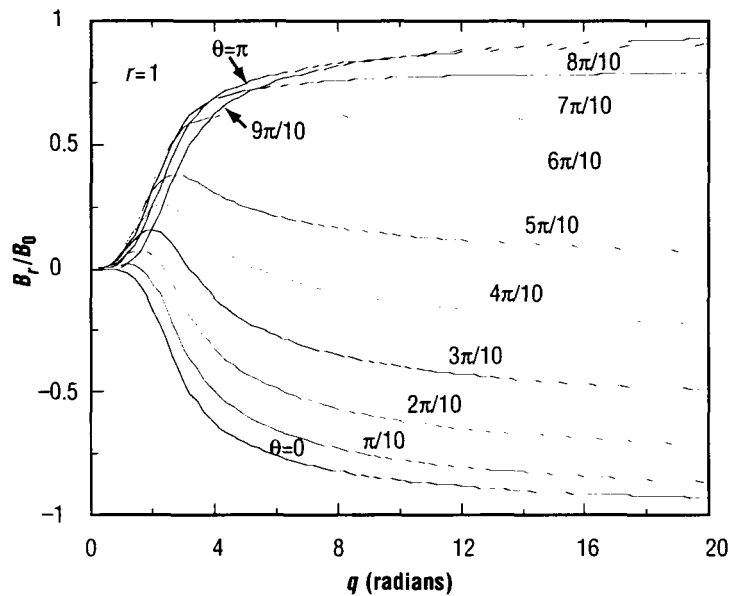


Figure 5. Dependence of the  $r$  component of the normalized magnetic field on the skin depth parameter,  $q$ , for several angular positions: 0, 0.5, 1, 1.5, 2, and  $p$ , in radians.

The presented model should give practically correct values at the center of the cylinder rim of the induced fields for the case of aspect ratio on the order of 10 or larger. Physically, for the high rotational rates, the fields at the center of the rim should also be given correctly by this model as the skin depth for the fields becomes small. Thus, the fields at the sidewalls will not overlap and will not penetrate to the middle zone. In other words, sidewall effects will not be present at this position. Plots of the magnetic field lines for different values of the skin depth parameter,  $q$ , are presented in figure 6. For small rotational speeds, the magnetic field penetrates through the metallic cylinder. As the speed increases, the lines are repelled from the center of the cylinder. Also, rotation of the lines is evident.

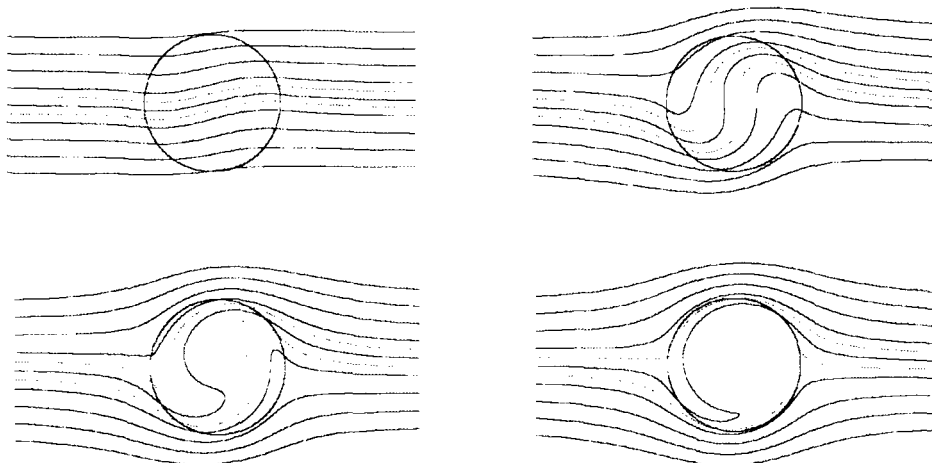


Figure 6. The streamlines of the total magnetic field for a set of the  $q$  values: 1, 3, 5, and 10. The external magnetic field goes from left to the right, and the wheel rotates counterclockwise. As the speed increases, the magnetic field is repelled from the wheel.

## 5. FINITE CYLINDER MODEL

In this section, we develop a theoretical magnetohydrodynamic model of a nonaxisymmetric Faraday disc of a finite length. We consider an electrically conducting solid cylinder with electrical conductivity,  $\sigma$ ; radius,  $r_0$ ; and height,  $2L$ . The cylinder rotates around its axis with the rotational velocity,  $\omega$ . An external uniform magnetic field of strength,  $B_0$ , is applied in a direction perpendicular to the cylinder axis. The geometry of the model as well as the cylindrical coordinate system used here is depicted in figure 7. We further assume that the external magnetic field is turned on sufficiently slow and the mechanical rotational accelerations are small. For this stationary case, we have

$$\nabla \times \mathbf{B} = \mu \mathbf{J}, \quad \mathbf{J} = \sigma(\mathbf{E} + \mathbf{v} \times \mathbf{B}), \quad \nabla \times \mathbf{E} = 0, \quad \nabla \cdot \mathbf{J} = 0, \quad \nabla \cdot \mathbf{B} = 0, \quad (8)$$

where  $\mathbf{B}$  is the magnetic field,  $\mathbf{J}$  is the electric current density,  $\mathbf{v}$  is the velocity of the medium, and  $\mathbf{E}$  is the electric field.

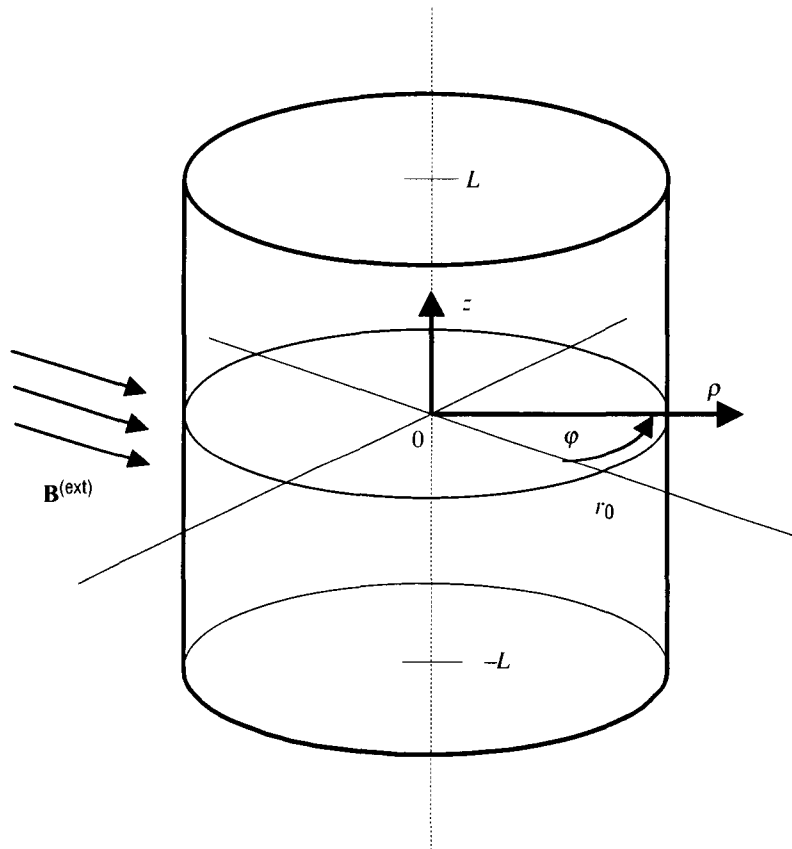


Figure 7. Schematic of the geometry and the cylindrical coordinates.

First, we eliminate the current from the equation for the magnetic field and obtain

$$\nabla \times \mathbf{B} = \mu\sigma(\mathbf{E} + \mathbf{v} \times \mathbf{B}) . \quad (9)$$

Further, in our case, the electric field can be expressed through the scalar potential,  $\Phi$ , as

$$\mathbf{E} = -\nabla\Phi . \quad (10)$$

The required velocity of the rigidly rotating cylinder is

$$\mathbf{v} = \omega r \mathbf{e}_\varphi . \quad (11)$$

At this point we introduce, for greater convenience, complex fields according to the following rule between the experimental  $\mathbf{B}^{(\text{exp})}$  and complex  $\mathbf{B}$  fields:

$$\mathbf{B}^{(\text{exp})} = \text{Re}[\mathbf{B}(r) \exp i\varphi] . \quad (12)$$

Then the externally applied uniform magnetic field, in its complex representation, is

$$\mathbf{B}^{(\text{ext})} = B_0 \mathbf{e}_r + iB_0 \mathbf{e}_\varphi , \quad (13)$$

and we have

$$\mathbf{v} \times \mathbf{B}^{(\text{ext})} = -\omega r B_0 \mathbf{e}_z . \quad (14)$$

Since the problem under consideration is linear, higher angular harmonics are not involved, and thus the angular derivatives can be replaced by the imaginary unity number  $\frac{\partial}{\partial\varphi} = i$  .

Also note, we are solving for the induced magnetic field that evidently drops to zero at distances sufficiently far from the spinning wheel. We scale distances by the radius of the cylinder and the electric potential by  $\omega r_0^2$ .

After simple algebra, we obtain from equations (8)–(10) the following set of governing equations:

$$\left[ \frac{\partial^2}{\partial r^2} + \frac{1}{r} \frac{\partial}{\partial r} - \frac{1}{r^2} + \frac{\partial^2}{\partial z^2} \right] B_z + q^2 B_z = 0 , \quad (15a)$$

where  $q^2 = -i\mu\sigma\omega r_0^2$  ,

$$\left[ \frac{\partial^2}{\partial r^2} + \frac{1}{r} \frac{\partial}{\partial r} - \frac{1}{r^2} + \frac{\partial^2}{\partial z^2} \right] \Phi + q^2 \Phi = 2B_z \quad (15b)$$

$$\frac{\partial B_r}{\partial z} = \frac{\partial B_z}{\partial r} + \frac{q^2}{r} \Phi, \quad \frac{\partial B_\phi}{\partial z} = \frac{i}{r} B_z + iq^2 \left( \frac{\partial \Phi}{\partial r} - rB_z \right) \quad (15c)$$

$$\frac{1}{r} \frac{\partial}{\partial r} (rB_\phi) - \frac{i}{r} B_r = -iq^2 \left( \frac{\partial \Phi}{\partial z} + rB_0 + rB_r \right). \quad (15d)$$

A general solution for equation (15a) is a superposition of the following functions:

$$B_z = C_1 \exp(\varepsilon z) J_1(kr), \quad k = \sqrt{\varepsilon^2 - i\mu\sigma\omega} = \sqrt{\varepsilon^2 + q^2}, \quad (16)$$

where  $C_1$  and  $\varepsilon$  are nonspecified at this moment.

This form, in turn, leads to the following solution for the potential,  $\Phi$ , and the rest of the field components:

$$\Phi = C_2 J_1(kr) - C_1 \frac{\omega r}{k} J_1'(kr) \quad (17a)$$

$$B_r = C_2 \frac{q^2}{\varepsilon \omega r} J_1(kr) + C_1 \frac{\varepsilon}{k} J_1'(kr) \quad (17b)$$

$$B_\phi = C_1 \frac{i\varepsilon}{k^2 r} J_1(kr) + C_2 \frac{iq^2 k}{\varepsilon \omega} J_1'(kr). \quad (17c)$$

Now, in order to obtain the required coefficients, we need to consider boundary conditions at the surface of the wheel. As the surrounding cylinder medium (air) is an electric insulator, the normal to the surface component of the electric current has to vanish. At the rim ( $r=1$ ), we should then have

$$-\frac{\partial \Phi}{\partial r} + rB_z = 0, \quad (18)$$

which gives us the relationship between  $C_1$  and  $C_2$  as

$$C_1 \omega J_1(k) = C_2 k^3 J_1'(k) \quad (19)$$

In principle, we have three sets of possible solutions:

$$\begin{aligned}
 (1) \quad C_1 &= C_2 \frac{k^3 J_1'(k)}{\omega J_1(k)} . \\
 (2) \quad C_1 &= 0, \quad J_1'(k) = 0 . \\
 (3) \quad C_2 &= 0, \quad J_1(k) = 0 .
 \end{aligned} \tag{20}$$

Cases (2) and (3) yield  $B_z(r=1)=0$ .

At the sidewalls ( $z=\pm L$ ), we have from the condition of  $J_z$  being zero there:

$$\frac{\partial \Phi}{\partial z} = -rB_0 - rB_r . \tag{21}$$

Finally, in order to write down the components of the magnetic fields as series expansions, we note that as a function of  $z$ ,  $B_r$ , and  $B_\phi$  are even, and  $\Phi$  and  $B_z$  are odd.

Below, we write down our general solution in terms of these three series expansions as outlined above.

First consider case (1). As the  $z$  component of the magnetic field is an odd function of  $z$ , then it is convenient to expand it into a Fourier sine series as

$$B_z^{(1)} = \sum_n D_n \frac{I_1(\lambda_n r)}{I_1(\lambda_n)} \sin p_n z , \tag{22a}$$

where  $\lambda_n^2 = p_n^2 - q^2$ ,  $p_n = \frac{\pi}{L} \left( n - \frac{1}{2} \right)$ ,  $n = 1, 2, 3, \dots$ . Also note that  $\cos(p_n L) = 0$  and  $\sin(p_n L) = (-1)^{n+1}$ .

The rest of the fields are

$$B_z^{(2)} = 0 \tag{22b}$$

$$B_\phi^{(1)} = -i \sum_n D_n \left[ \frac{p_n I_1(\lambda_n r)}{\lambda_n^2 r I_1(\lambda_n)} + \frac{q^2 I_1'(\lambda_n r)}{\lambda_n^2 p_n I_1'(\lambda_n)} \right] \cos p_n z \tag{22c}$$

$$B_r^{(1)} = - \sum_n D_n \left[ \frac{q^2 I_1(\lambda_n r)}{p_n \lambda_n^3 I_1'(\lambda_n) r} + \frac{p_n I_1'(\lambda_n r)}{\lambda_n I_1(\lambda_n)} \right] \cos p_n z \tag{22d}$$

$$\Phi^{(1)} = \sum D_n \left( \frac{I_1(\lambda_n r)}{\lambda_n^3 I_1'(\lambda_n)} + \frac{r}{\lambda_n} \frac{I_1'(\lambda_n r)}{I_1(\lambda_n)} \right) \sin(p_n z). \quad (22e)$$

Consider now case (2), corresponding to the solution with no  $z$  component of the magnetic field. This set also includes the  $z$  independent term. We have

$$B_z^{(2)} = 0 \quad (23a)$$

$$B_\phi^{(2)} = \sum A_n \frac{iq^2 \kappa_n}{\varepsilon_n} \frac{J_1'(\kappa_n r)}{J_1(\kappa_n)} \frac{\cosh(\varepsilon_n z)}{\cosh(\varepsilon_n L)} + B_{0\phi} \quad (23b)$$

$$B_r^{(2)} = \sum A_n \frac{q^2}{\varepsilon_n r} \frac{J_1(\kappa_n r)}{J_1(\kappa_n)} \frac{\cosh(\varepsilon_n z)}{\cosh(\varepsilon_n L)} + B_{0r} \quad (23c)$$

$$\Phi^{(2)} = \sum A_n \frac{J_1(\kappa_n r)}{J_1(\kappa_n)} \frac{\sinh(\varepsilon_n z)}{\cosh(\varepsilon_n L)}, \quad (23d)$$

where we have

$$B_{0r} = -B_0 + C_0 J_1(qr) / r, \quad B_{0\phi} = -iB_0 + iC_0 q J_1'(qr). \quad (24)$$

From the boundary condition equation (21) at  $z=L$ ,

$$\sum_n A_n \frac{\kappa_n^2}{\varepsilon_n} \frac{J_1(\kappa_n r)}{J_1(\kappa_n)} + C_0 J_1(qr) = 0. \quad (25)$$

This equation can be readily solved yielding coefficients

$$A_n = -\frac{2C_0 \varepsilon_n q J_1'(q) J_1(\kappa_n)}{(\kappa_n^2 - 1)(\kappa_n^2 - q^2) \kappa_n J_0(\kappa_n)}. \quad (26)$$

Note that  $B_{2\phi}(r,L) = B_{2\phi}(1,z) = B_{0\phi}(1)$  and  $B_{2r}(r,L) = iB_{0\phi}(1)$ .

Consider now a set corresponding to the case (3). Let

$$J_1(\beta_n) = 0, \quad \gamma_n = \sqrt{\beta_n^2 - q^2} . \quad (27)$$

Then the associated solution of equation (15) is

$$B_z^{(3)} = \sum_n C_n \frac{J_1(\beta_n r) \sinh(\gamma_n z)}{J_0(\beta_n) \cosh(\gamma_n L)} \quad (28a)$$

$$B_\phi^{(3)} = \sum_n C_n \frac{i\gamma_n J_1(\beta_n r) \cosh(\gamma_n z)}{\beta_n^2 r J_0(\beta_n) \cosh(\gamma_n L)} \quad (28b)$$

$$B_r^{(3)} = \sum_n C_n \frac{\gamma_n J_1'(\beta_n r) \cosh(\gamma_n z)}{\beta_n J_0(\beta_n) \cosh(\gamma_n L)} \quad (28c)$$

$$\Phi^{(3)} = -\sum_n C_n \frac{r J_1'(\beta_n r) \sinh(\gamma_n z)}{\beta_n J_0(\beta_n) \cosh(\gamma_n L)} . \quad (28d)$$

At this point the boundary conditions for the electric current are fulfilled exactly, but the solution is still not fully specified, as the coefficients  $C_n$  and  $D_n$  are arbitrary and not defined. The remaining condition on the solution of our problem comes from the far-field condition of the vanishing solution at infinity. This condition is nontrivial, as it requires formulating a solution in the free region outside the medium and matching it at the boundaries. In order to avoid this, a surface integral formalism can be invoked instead. Indeed, outside the medium, the magnetostatic equations can be used and thus the theory of a scalar potential can be applied. We consider a potential,  $u$ , that satisfies the Laplace equation:

$$u(\mathbf{r}) = u(\rho, z) e^{i\phi}, \quad \nabla^2 u = 0 . \quad (29)$$

Then, in free space, the magnetic field components can be represented as

$$\frac{\partial u}{\partial z} = B_z, \quad \frac{\partial u}{\partial r} = B_r, \quad u = -i\rho B_\phi . \quad (30)$$

From the Green theorem,

$$\Omega u(\rho_0, z_0) = \oint_S \left( \frac{\partial u(\rho, z)}{\partial n} - u(\rho, z) \frac{\partial}{\partial n} \right) \frac{1}{|\mathbf{r} - \mathbf{r}_0|} e^{i(\phi - \phi_0)} dS, \quad (31)$$

where  $\Omega = 4\pi$  if  $r_0$  belongs to the region surrounded by the surface,  $S$ , otherwise  $\Omega$  is zero.

Integration over the angular variable can be readily performed, leading to the cylindrical Green function, which can be represented in this particular form:

$$G = 2\pi \int_0^{\infty} J_1(k\rho) J_1(k\rho_0) e^{-k|z-z_0|} dk . \quad (32)$$

For our geometry, we obtain from equation (31)

$$\begin{aligned} \Omega u(\rho_0 z_0) = & - \int_{-L}^L dz r_0 \left[ \frac{\partial}{\partial \rho} u(\rho z) - u(\rho z) \frac{\partial}{\partial \rho} \right] G(\rho z \rho_0 z_0) \Big|_{\rho=r_0} \\ & + \int_0^{r_0} \rho d\rho \left[ \frac{\partial}{\partial z} u(\rho z) - u(\rho z) \frac{\partial}{\partial z} \right] G(\rho z \rho_0 z_0) \Big|_{z=-L} \\ & - \int_0^{r_0} \rho d\rho \left[ \frac{\partial}{\partial z} u(\rho z) - u(\rho z) \frac{\partial}{\partial z} \right] G(\rho z \rho_0 z_0) \Big|_{z=L} . \end{aligned} \quad (33)$$

In terms of the magnetic field components, we have

$$\begin{aligned} -4\pi i \rho_0 B_\varphi(\rho_0 z_0) = & - \int_{-L}^L dz \left[ B_r(1z) G(1z \rho_0 z_0) + i B_\varphi(1z) \frac{\partial G}{\partial \rho}(\rho=1, z \rho_0 z_0) \right] \\ & + \int_0^1 \rho d\rho B_z(\rho, -L) [G(\rho, -L, \rho_0 z_0) + G(\rho L \rho_0 z_0)] \\ & + i \int_0^1 \rho^2 d\rho B_\varphi(\rho, -L) \frac{\partial}{\partial z} [G(\rho, z=-L, \rho_0 z_0) - G(\rho, z=L, \rho_0 z_0)] , \end{aligned} \quad (34)$$

where the parity properties of the fields were already taken into account. In the above expression, the observation point  $r_0$  is outside the medium region. When it approaches the surface from outside, the condition for the unknown coefficients  $C_n$  and  $D_n$  results. Below, the two surfaces of the cylinder will be treated separately. We first consider the sidewall. In this case,  $z_0 = -L - \varepsilon$ ,  $0 < r_0 < 1$ , where  $\varepsilon$  is infinitesimally small. Using the Bessel function representation for the Green function, equation (32), we can put equation (34) into the following convenient form:

$$-i\rho_0 B_\varphi(\rho_0 L) = \int_0^\infty dk J_1(k\rho_0) \Pi(kL), \quad (35)$$

where

$$\begin{aligned} \Pi(kL) = & - \int_{-L}^L dz \left[ B_r(1z) J_1(k) + i B_\varphi(1z) k J_1'(k) \right] e^{-k(z+L)} \\ & - \left( e^{-2kL} + 1 \right) \int_0^1 \rho d\rho J_1(k\rho) B_z(\rho L) \\ & + i k e^{-2kL} \int_0^1 \rho^2 d\rho J_1(k\rho) B_\varphi(\rho L). \end{aligned} \quad (36)$$

Now we multiply both sides of equation (35) by  $\int_0^1 \rho_0 J_1(\beta_m \rho_0) d\rho_0$  and get

$$C_m \frac{\gamma_m}{2\beta_m^3} + \frac{1}{\beta_m^2} i B_{0\varphi}(1) = \int_0^\infty dk \frac{J_1(k)}{k^2 - \beta_m^2} \Pi(kL). \quad (37)$$

The resulting expression involves a number of auxiliary matrices that can be evaluated numerically. These can be presented as follows:

$$G_{mn}^{(i)} = \int_0^\infty dk \frac{J_1(k)}{k^2 - \beta_m^2} G_n^{(i)}, \quad (38)$$

where

$$G_n^{(1)} = \frac{k J_1(k)}{k^2 - \beta_n^2} e^{-2kL}, \quad G_n^{(2)} = \frac{J_1(k)}{k^2 - \beta_n^2} (1 + e^{-2kL}), \quad G_n^{(3)} = \frac{k J_1(k)}{k^2 - \gamma_n^2} (1 - e^{-2kL}),$$

$$G_n^{(4)} = \frac{J_1(k)}{k^2 - \gamma_n^2} (1 + e^{-2kL}), \quad G_n^{(5)} = \frac{\lambda_n I_0(\lambda_n) J_1(k) - I_1(\lambda_n) k J_0(k)}{(k^2 + \lambda_n^2) I_1(\lambda_n)} (1 + e^{-2kL}),$$

$$G_n^{(6)} = \frac{J_1(k)}{k^2 + p_n^2} (1 + e^{-2kL}), \quad G_n^{(7)} = \frac{kJ_0(k)}{k^2 + p_n^2} (1 + e^{-2kL}), \quad G_n^{(9)} = \frac{kJ_1(k)}{k^2 - \varepsilon_n^2} (1 - e^{-2kL}),$$

$$G_n^{(10)} = \frac{J_1(k)}{k^2 - \varepsilon_n^2} (1 + e^{-2kL}), \quad \text{and} \quad g_m^{(1)} = \int_0^\infty \frac{J_1^2(k)}{k(k^2 - \beta_m^2)} e^{-2kL} dk. \quad (38a)$$

Now we define principal matrices:

$$M_{m,n} = \frac{\gamma_n}{2\beta_n^3} \delta_{m,n} + \frac{\gamma_n}{\beta_n} (G_{mn}^{(1)} + G_{mn}^{(3)}) + \tanh(\gamma_n L) \left( \beta_n G_{mn}^{(2)} - \frac{\gamma_n^2}{\beta_n} G_{mn}^{(4)} \right) \quad (39a)$$

$$\bar{N}_{m,n} = (-1)^n \left[ G_{mn}^{(5)} + \frac{p_n^2 + q^2}{\lambda_n^2} (G_{mn}^{(7)} - G_{mn}^{(6)}) - s_n p_n G_{mn}^{(6)} \right] \quad (39b)$$

$$F_m = -\frac{iB_{0\varphi}(1)}{\beta_m^2} + B_{0r}(1) \left( g_m^{(1)} + \frac{1}{2\beta_m^2} \right) + iB_{0\varphi}(1) \left( g_m^{(1)} - \frac{1}{2\beta_m^2} \right)$$

$$- \sum A_n \frac{q^2}{\varepsilon_n} \left[ G_{mn}^{(9)} - G_{mn}^{(10)} \varepsilon_n \tanh(\varepsilon_n L) \right], \quad (39c)$$

where

$$s_n = \frac{q^2 I_1(\lambda_n)}{p_n \lambda_n^3 I_1'(\lambda_n)} + \frac{p_n I_1'(\lambda_n)}{\lambda_n I_1(\lambda_n)}. \quad (40)$$

We end up now with the matrix equation

$$[\mathbf{M}]\mathbf{C} = \mathbf{F} + [\mathbf{N}]\mathbf{D}. \quad (41)$$

Now consider the case of  $r=1, -L < z < L$ . We have from equation (34)

$$-2iB_\varphi(1z_0) = \int_0^\infty dk J_1(k) \Pi(kz_0), \quad (42)$$

where

$$\begin{aligned} \Pi(kz_0) = & - \int_{-L}^L dz \left[ B_r(1z)J_1(k) + iB_\varphi(1z)kJ_1'(k) \right] e^{-k|z-z_0|} \\ & + e^{-kL} \left( e^{kz_0} + e^{-kz_0} \right) \int_0^1 \rho d\rho J_1(k\rho) \left[ ik\rho B_\varphi(\rho L) - B_z(\rho L) \right]. \end{aligned} \quad (43)$$

In order to assure for a fast Fourier cosine series convergence, we need to extract the constant term from both sides:

$$-2i \left[ B_\varphi(1z_0) - B_\varphi(1L) \right] = \int_0^\infty dk J_1(k) \left[ \Pi(kz_0) - \Pi(kL) \right]. \quad (44)$$

Then the cosine series expansion gives

$$-D_m \frac{2L}{p_m} \frac{p_m^2 + q^2}{\lambda_m^2} = \int_{-L}^L dz \cos(p_m z) \int_0^\infty dk J_1(k) \left[ \Pi(kz_0) - \Pi(kL) \right]. \quad (45)$$

After considerable algebra, this expression can be put into a matrix form. For convenience, we introduce a set of matrices, which can be numerically evaluated and are  $t_m^{(i)} = \int_0^\infty dk J_1(k) t^{(i)}$ , where

$$\begin{aligned} t^{(1)} &= \frac{kJ_1(k)}{k^2 + p_m^2}, \quad t^{(2)} = \frac{(1 - e^{-2kL})J_1(k)}{k(k^2 + p_m^2)}, \quad t^{(3)} = \frac{k^2 J_1'(k)}{k^2 + p_m^2}, \\ t^{(4)} &= \frac{(1 + e^{-2kL})J_1(k)}{k(k^2 + p_m^2)}, \quad t^{(5)} = \frac{(1 - e^{-2kL})J_1'(k)}{k^2 + p_m^2}, \quad t^{(6)} = \frac{k^2(1 + e^{-2kL})J_2(k)}{k^2 + p_m^2}, \\ t^{(7)} &= \frac{k(1 + e^{-2kL})J_1'(k)}{k^2 + p_m^2}, \quad \text{and} \quad t^{(8)} = \frac{(1 - e^{-2kL})J_1(k)}{(k^2 + p_m^2)}, \end{aligned} \quad (46a)$$

and, similarly  $T_{m,n}^{(i)} = \int_0^\infty dk J_1(k^+) T^{(i)}$ , where

$$\begin{aligned}
T^{(1)} &= \frac{(1+e^{-2kL})J_1(k)}{(k^2+p_m^2)(k^2+p_n^2)}, \quad T^{(2)} = \frac{(1+e^{-2kL})kJ_1'(k)}{(k^2+p_m^2)(k^2+p_n^2)}, \\
T^{(3)} &= \frac{k^2(1+e^{-2kL})}{(k^2+p_m^2)} \frac{\lambda_n I_0(\lambda_n)J_1(k) - I_1(\lambda_n)kJ_0(k)}{(k^2+\lambda_n^2)I_1(\lambda_n)}, \\
T^{(4)} &= \frac{(1+e^{-2kL})k^3J_1(k)}{(k^2+p_m^2)(k^2-\beta_n^2)}, \quad T^{(5)} = \frac{(1+e^{-2kL})k^2J_1(k)}{(k^2+p_m^2)(k^2-\beta_n^2)}, \\
T^{(6)} &= \frac{(1+e^{-2kL})k^2J_1(k)}{(k^2+p_m^2)(k^2-\gamma_n^2)}, \quad T^{(7)} = \frac{(1-e^{-2kL})k^3J_1(k)}{(k^2+p_m^2)(k^2-\gamma_n^2)}, \\
T^{(8)} &= \frac{(1+e^{-2kL})J_1(k)k^2}{(k^2+p_m^2)(k^2-\epsilon_n^2)}, \quad \text{and } T^{(9)} = \frac{(1-e^{-2kL})k^3J_1(k)}{(k^2+p_m^2)(k^2-\epsilon_n^2)}. \tag{46b}
\end{aligned}$$

We now introduce the following matrices:

$$\begin{aligned}
U_{mn} &= 2L \left( \frac{1-t_m^3}{p_m} \frac{p_m^2+q^2}{\lambda_m^2} + s_m t_m^{(1)} \right) \delta_{mn} \\
&\quad - 2s_n p_m (-1)^{m+n+1} \left( p_n T_{mn}^{(1)} - \frac{t_n^{(8)}}{p_m} \right) \\
&\quad + 2(-1)^{m+n+1} \frac{p_n^2+q^2}{\lambda_n^2} \left[ p_m T_{mn}^{(2)} - \frac{t_n^{(7)}}{p_m} \right], \tag{47a}
\end{aligned}$$

$$V_{mn} = -2(-1)^m \frac{\gamma_n}{p_m \beta_n} \left[ -\frac{2p_m^2 t_m^{(1)}}{\gamma_n^2 + p_m^2} + T_{mn}^{(4)} + T_{mn}^{(7)} + \tanh(\gamma_n L) \left( \frac{\beta_n^2}{\gamma_n} T_{mn}^{(5)} - \gamma_n T_{mn}^{(6)} \right) \right], \tag{47b}$$

$$\begin{aligned}
E_m = & B_{0r}(1)(-1)^{m+1} \left( 2p_m t_m^{(2)} + \frac{4t_m^{(1)}}{p_m} \right) \\
& + iB_{0\phi}(1)(-1)^{m+1} \left( 2p_m t_m^{(5)} + \frac{4(t_m^{(3)} - 1)}{p_m} - 2p_m t_m^{(6)} \right) \\
& - \sum A_n p_m (-1)^m \frac{2q^2}{\epsilon_n w} \left[ \frac{2t_m^{(1)}}{\epsilon_n^2 + p_m^2} + \epsilon_n \tanh(\epsilon_n L) T_{mn}^{(7)} - T_{mn}^{(8)} \right]. \quad (47c)
\end{aligned}$$

Then the second matrix equation is

$$[\mathbf{U}]\mathbf{D} + [\mathbf{V}]\mathbf{C} = \mathbf{E}. \quad (48)$$

Combining this equation with equation (41), we obtain

$$\{[\mathbf{U}] + [\mathbf{V}][\mathbf{M}]^{-1}[\mathbf{N}]\}\mathbf{D} = \mathbf{E} - [\mathbf{V}][\mathbf{M}]^{-1}\mathbf{F}. \quad (49)$$

This matrix equation can be readily numerically inverted to yield the required values for vectors  $D$  and  $C$ . The required value  $C_0$  can be obtained from the condition of zeroing the last  $C_n$  coefficient. This condition makes the solution nonsingular by selecting the proper value for the  $z$ -independent term.

## 6. NUMERICAL RESULTS

In this section, we present the results of our numerical calculations based on the previous section. The aspect ratio is selected to be  $1/2$ , which is close to our experimental value. The other relevant nondimensional parameter is  $|q|$ , which is proportional to the square root of the rotational speed. The dependence of the magnetic field on this parameter is needed for comparisons with the experiment. For illustration purposes, we present below a set of six graphs for three components of the field within the cylinder boundaries, each component having the real and the imaginary part (fig. 8). The graphs are given for  $q = \sqrt{-i}$ . The rank of the matrices entering equations (41) and (49) was selected to be 10. This number is rather small, but gives sufficient accuracy for this electromagnetic problem ( $10^{-3}$ ). As expected, the  $B_z$  component vanishes at the center of the cylinder. The  $B_r$  value is largest at the middle of the rim, considering that we look only at the surface points.

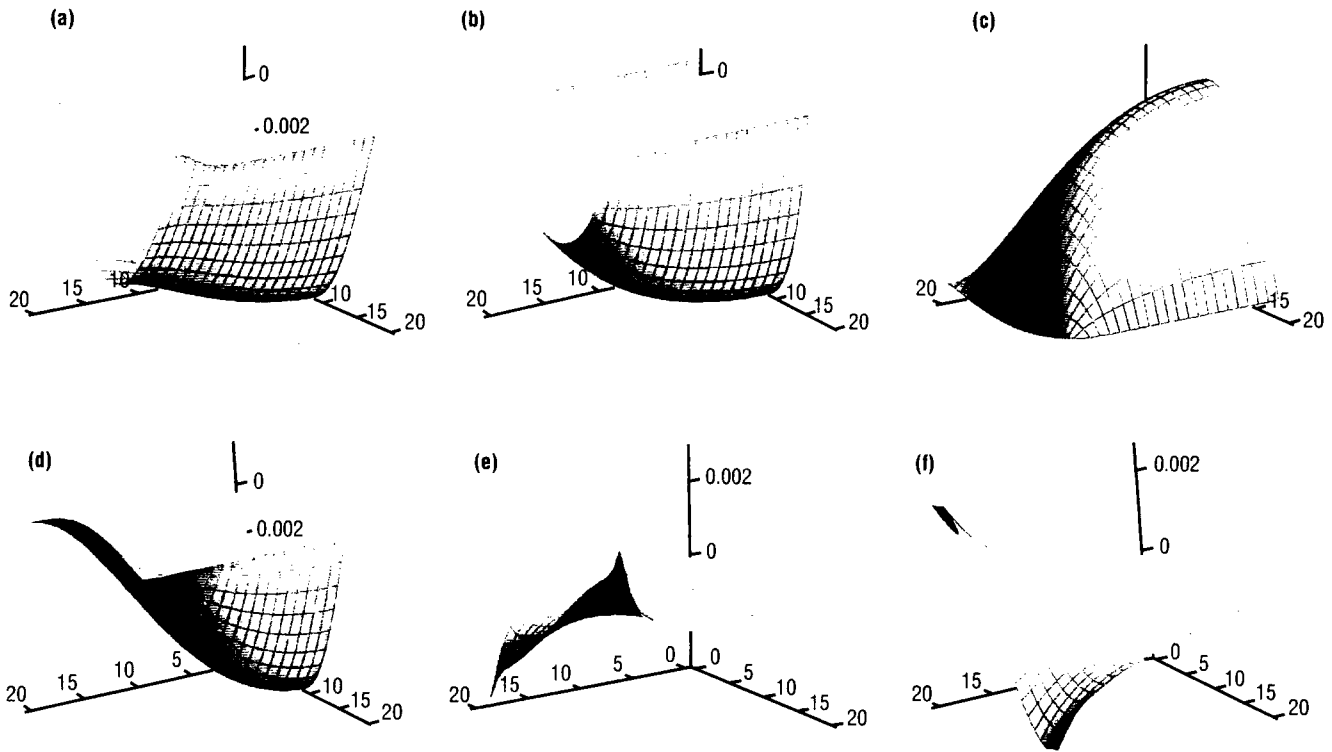


Figure 8. A set of six functions of  $r$  and  $z$  variables that represent the magnetic field in the spinning cylinder: (a)  $\text{Re}(B_r)$ , (b)  $\text{Im}(B_r)$ , (c)  $\text{Re}(B_j)$ , (d)  $\text{Im}(B_j)$ , (e)  $\text{Re}(B_z)$  and (f)  $\text{Im}(B_z)$ . Re is the real part and Im is the imaginary part.

Our numerical analysis shows a high degree of diagonality of the matrix  $\mathbf{M}$ . This was observed for practically all investigated  $L$  and  $q$  parameters. The nondiagonal elements are approximately five orders of magnitude smaller than the corresponding diagonal element. This feature can be exploited to obtain good analytical formulas, as the inversion of  $\mathbf{M}$  can be accomplished analytically with high accuracy. Similarly, the governing matrix in equation (49) is highly diagonal as well (at least three orders of magnitude difference). Figures 9 and 10 represent the  $B_r$  and  $B_\phi$  fields taken at the middle of the rim at several different angular positions. As expected, the qualitative behavior is the same as in the case of an infinitely long cylinder. The difference is in the position of the maximum for angles in vicinity of  $90^\circ$ . Specifically, the peak shifts toward the higher  $q$  values.

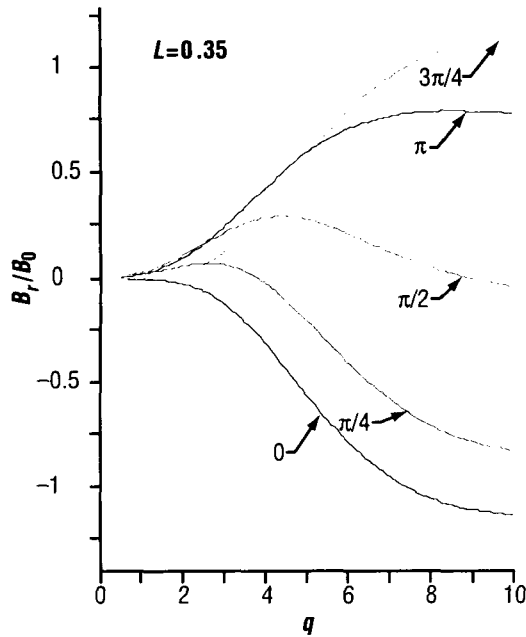


Figure 9.  $B_r/B_0$  as a function of the skin depth parameter,  $q$ . Values are taken at the middle of the rim.

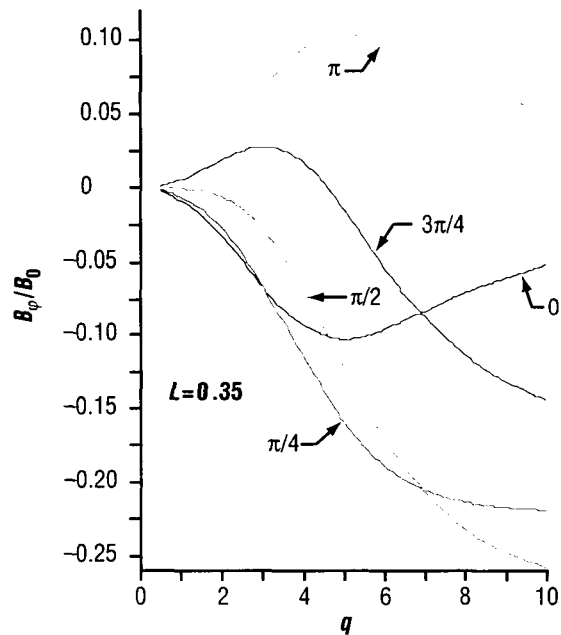


Figure 10.  $B_\phi/B_0$  as a function of the skin depth parameter,  $q$ . Values are taken at the middle of the rim.

## 7. EXPERIMENTAL RESULTS

A brass (copper+zinc) wheel, with a 4-in diameter and 1.4 in thick, was used for this investigation. Ceramic ball bearings were used to safely spin the wheel up to 40,000 rpm. The wheel was also electrically insulated from the rest of the armature. For spinning, an air turbine was used. The rotational velocity was measured by two methods: (1) A simple strobe light and (2) a photodiode that detected laser beam pulses as they passed through a slot in the rotating shaft. The magnetic sensor is based on a giant magnetoresistivity, and consists of a balanced bridge circuitry. The position of the sensor was as close as possible to the rim of the wheel. The linear dimension of the sensor is  $\approx 8$  mm so that the offset from the surface is on the order of 15 percent. We did not use any goniometer system, so the accuracy of the angular position is not high, being estimated within a few degrees, with the main uncertainty being the direction of Earth's magnetic field. We attempted to fit the experimental data with the presented theory by selecting the best value for the electrical conductivity of the wheel. The results of this procedure are displayed in figure 11, where the black dots represent experimental values. A slight misfit on the right shoulder can be due to slight angular misalignment from a  $90^\circ$  position. The obtained value for the resistivity is  $43$  n $\Omega$ m, which compares well with those listed in table 1. We can conclude, based on these measurements, that the proposed theory satisfactorily explains our experiments.

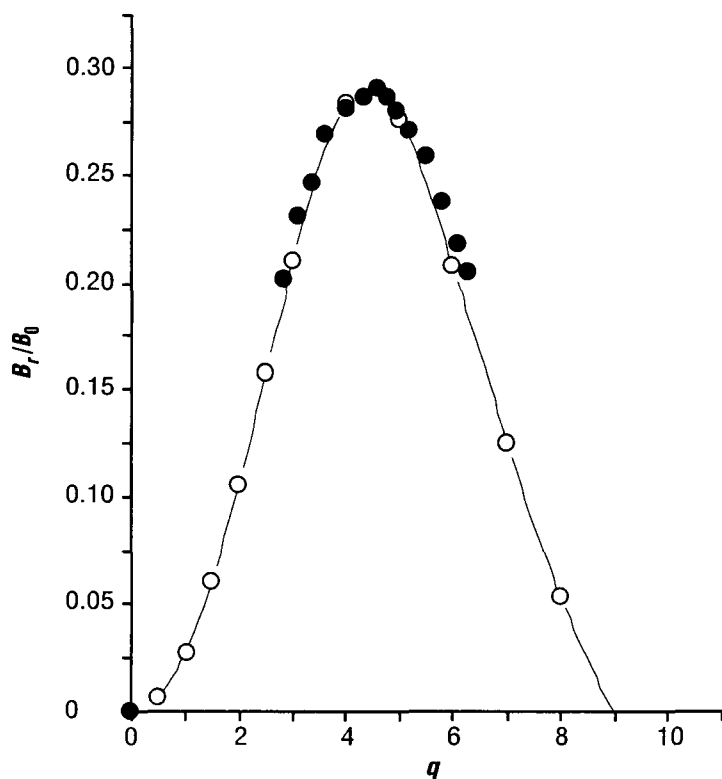


Figure 11. Experimental values (black circles) and the corresponding theoretical fit (hollow circles) assuming that the electrical conductivity is  $43$  n $\Omega$ m.

Table 1. Measured electrical resistivities for several brasses.

<b>Designation</b>	<b>Composition</b>	<b>Electrical Resistivity (nΩm)</b>
C21000	95 Cu – 5 Zn	31
C22000	90 Cu – 10 Zn	39.1
C22600	87.5 Cu – 12.5 Zn	43
C23000	85 Cu – 15 Zn	47
C24000	80 Cu – 20 Zn	54

## REFERENCES

1. Wheeler, J.A.: *Geometrodynamics*, Academic Press, NY, p. 1203, 1962.
2. Lamoreaux, S.K.: "Demonstration of the Casimir Force in the 0.6 to 6 Micron Range," *Phys. Rev. Lett.*, Vol. 78, No. 1, pp. 5–8, 1997.
3. Misner, C.W.; Thorne, K.S.; and Wheeler, J.A.: *Gravitation*, Freeman Publishing, San Francisco, pp. 114–119, 1973.
4. Braginsky, V.; Polnarev, A.; and Thorne, K.: "Foucault Pendulum at the South Pole: Proposal for an Experiment to Detect the Earth's General Relativistic Gravitomagnetic Field," *Phys. Rev. Lett.*, Vol. 53, No. 9, p. 863, 1984.
5. Bedford, D.; and Krum, P.: "On Relativistic Gravitation," *Amer. J. of Phys.*, Vol. 53, No. 9, pp. 889–890, 1985.
6. Krum, P.; and Bedford, D.: "The Gravitational Poynting Vector and Energy Transfer," *Amer. J. of Phys.*, Vol. 55, No. 4, pp. 362–363, 1987.
7. Mashhoon, B.; Paik, H.J.; and Will, C.: "Detection of the Gravitomagnetic Field Using an Orbiting Superconducting Gravity Gradiometer, Theoretical Principles," *Phys. Rev. D*, Vol. 39, No. 10, p. 2825, 1989.
8. Harris, E.: "Analog Between General Relativity and Electromagnetism for Slowly Moving Particles in Weak Gravitational Fields," *Amer. J. of Phys.*, Vol. 59, No. 5, pp. 421–425, 1991.
9. Myshkin, N.P.: "The Movement of an Object Placed in the Radiant Energy Flow," *Zh. Russ. Fiz.-Khim. Obshch.*, No. 3, p. 149, 1906.
10. Myshkin, N.P.: *Zh. Russ. Fiz.-Khim. Obshch.*, No. 6, 1911.
11. Kozyrev, N.A.; and Nasonov V.V.: "On Some Properties of Time Discovered By Astronomical Observations," *Problems of Analysis of the Universe* (in Russian), No. 9, p. 76, 1980.
12. Hayasaka, H.; and Takeuchi, S.: "Anomalous Weight Reduction on a Gyroscope's Right Rotations Around the Vertical Axis of the Earth," *Phys. Rev. Lett.*, Vol. 63, No. 9, p. 2701, 1989.
13. Nitschke, J.M.; and Wilmarth, P.A.: "Null Result for the Weight Change of a Spinning Gyroscope," *Phys. Rev. Lett.*, Vol. 64, No. 18, pp. 2115–2116, 1989.

14. Quinn, T.J.; and Picard, A.: "The Mass of Spinning Rotors: No Dependence on Speed or Sense of Rotation," *Nature*, Vol. 343, February 22, p. 2115, 1990.
15. Salter, S.H.: "Good Vibrations for Physics," *Nature*, Vol. 343, February 8, p. 509, 1990.
16. Shipov, G.I.: "On Using of Vacuum Torsion Fields for Movement of Mechanical Systems," *CISE VENT*, preprint No. 8 (in Russian), Moscow, p. 50, 1991.
17. Gerber, K.; Merit, R.F.; and Delves, E.: "Gyro Drop Experiment," [www.ourhollowearth.com/Gyro.htm](http://www.ourhollowearth.com/Gyro.htm), August 1999.
18. Brush, C.F.: "Discussion of a Kinetic Theory of Gravitation II; and Some New Experiments in Gravitation," *Proc. Amer. Phil. Soc.*, Vol. LX, p. 23, 1921.
19. Brush, C.F.: "Discussion of a Kinetic Theory of Gravitation II; and Some New Experiments in Gravitation—Second Paper," *Proc. Amer. Phil. Soc.*, Vol. LXI, p. 167, 1922.
20. Brush, C.F.: "Discussion of a Kinetic Theory of Gravitation II; and Some New Experiments in Gravitation—Third Paper," *Proc. Amer. Phil. Soc.*, Vol. LXII, D, p. 75, 1923.
21. Wallace, H.M.: "Method and Apparatus For Generating a Secondary Gravitational Force Field," U.S. Patent No. 3266605, December 14, 1971.
22. Wallace, H.M.: "Method and Apparatus For Generating a Dynamic Force Field," U.S. Patent No. 3626606, December 14, 1971.
23. Wallace, H.M.: "Heat Pump," U.S. Patent No. 3823570, July 16, 1974.
24. Hoyle, C.D.; Schmidt, U.; Heckel, B.R.; et al.: "Sub-millimeter Test of the Gravitational Inverse-Square Law: A, Search for "Large" Extra Dimensions," *Phys. Rev. Lett.* Vol. 86, p. 1418, 2001.
25. *Metals Handbook*, Ninth Edition, Volume 2, Properties and Selection: Nonferrous Alloys and Pure Metals, American Society for Metals, 1979.

REPORT DOCUMENTATION PAGE			Form Approved OMB No. 0704-0188	
Public reporting burden for this collection of information is estimated to average 1 hour per response, including the time for reviewing instructions, searching existing data sources, gathering and maintaining the data needed, and completing and reviewing the collection of information. Send comments regarding this burden estimate or any other aspect of this collection of information, including suggestions for reducing this burden, to Washington Headquarters Services, Directorate for Information Operation and Reports, 1215 Jefferson Davis Highway, Suite 1204, Arlington, VA 22202-4302, and to the Office of Management and Budget, Paperwork Reduction Project (0704-0188), Washington, DC 20503				
1. AGENCY USE ONLY (Leave Blank)	2. REPORT DATE February 2003	3. REPORT TYPE AND DATES COVERED Technical Memorandum		
4. TITLE AND SUBTITLE An Experimental Investigation To Determine Interaction Between Rotating Bodies (MSFC Center Director's Discretionary Fund Final Report, Project No. 279-00-16)			5. FUNDING NUMBERS	
6. AUTHORS R.N. Grugel, M.P Volz, and K. Mazuruk*				
7. PERFORMING ORGANIZATION NAMES(S) AND ADDRESS(ES) George C. Marshall Space Flight Center Marshall Space Flight Center, AL 35812			8. PERFORMING ORGANIZATION REPORT NUMBER  M-1065	
9. SPONSORING/MONITORING AGENCY NAME(S) AND ADDRESS(ES) National Aeronautics and Space Administration Washington, DC 20546-0001			10. SPONSORING/MONITORING AGENCY REPORT NUMBER NASA/TM-2003-212286	
11. SUPPLEMENTARY NOTES *Universities Space Research Association, Huntsville, AL Prepared by Microgravity Science and Applications Department, Science Directorate				
12a. DISTRIBUTION/AVAILABILITY STATEMENT Unclassified-Unlimited Subject Category 72 Nonstandard Distribution			12b. DISTRIBUTION CODE	
13. ABSTRACT (Maximum 200 words)  A number of recent advanced theories related to torsion properties of the space-time matrix predict the existence of an interaction between classically spinning objects. Indeed, some experimental data suggest that spinning magnetic bodies discernibly interact with Earth's natural fields. If a rotating body modifies the geometry of space-time, then nuclear spins could be used for detection. Thus, assuming a spinning body induces a torsion field, a sensor based on the giant magnetoresistance effect would detect local changes. Experimentally, spinning a brass wheel shielded from Earth's magnetic field showed no measurable change in signals; without shielding, a Faraday disc phenomenon was observed. Unexpected experimental measurements from the nonaxial Faraday disc configuration were recorded, and a theoretical model was derived to explain them.				
14. SUBJECT TERMS Faraday disc, magnetic field, rotating bodies			15. NUMBER OF PAGES 40	
			16. PRICE CODE	
17. SECURITY CLASSIFICATION OF REPORT Unclassified	18. SECURITY CLASSIFICATION OF THIS PAGE Unclassified	19. SECURITY CLASSIFICATION OF ABSTRACT Unclassified	20. LIMITATION OF ABSTRACT Unlimited	